Development of Hard-Turbulent Convection in Two Dimensions: Numerical Evidence

J. Werne,[1] E. E. DeLuca,[2] R. Rosner,[1] and F. Cattaneo[1]
[1]*Enrico Fermi Institute, The University of Chicago, Chicago, Illinois 60637*
[2]*Institute for Astronomy, University of Hawaii, Honolulu, Hawaii 96822*
(Received 19 February 1991)

New numerical evidence for a transition to hard turbulence in 2D Boussinesq convection is presented. These 2D simulations agree with some, but not all, experimental results for the scaling properties of 3D hard turbulence. The transition to 2D hard turbulence, as measured by a change in the Nusselt-Rayleigh scaling law, coincides with a gradual change in the velocity probability distribution from Gaussian to exponential form and with the development of a "well-mixed" central region.

PACS numbers: 47.25.Ae, 47.25.Qv

Experiments of unit-aspect-ratio Rayleigh-Bénard convection conducted at The University of Chicago [1–4] have characterized a previously unknown regime of turbulent convection. The major aspects of this confined flow include the following: (i) the emergence of a robust roll characterized by a mean vertical sidewall velocity V_s directed oppositely on either side of the cell, a horizontal temperature gradient Δ_x/L, and a coherence frequency ω_p, signaling an overall organization of the flow with a particular time scale; (ii) a characteristic temperature scale Δ_c for fluctuations in the central region of the cell; and (iii) a deviation in the power-law dependence of the convective heat transport, $\mathrm{Nu}-1$, from the "classical" index of $\frac{1}{3}$ [5]. Indeed, a distinguishing feature of this flow is the scaling exhibited by each of these quantities with the Rayleigh number R. The measured values for the scaling indices are as follows [2,3]: $\mathrm{Nu}-1\propto R^{\alpha}$, $\alpha=0.282\pm0.006$; $\Delta_c\propto R^{\beta}$, $\beta=-0.147\pm0.005$; $\omega_p\propto R^{\gamma}$, $\gamma=0.491\pm0.002$; $V_s\propto R^{\delta}$, $\delta=0.485\pm0.005$; $\Delta_x\propto R^{\epsilon}$, $\epsilon=\beta$. Additional features of this "hard turbulence" include the existence of coherent structures in the flow, manifested as thermal plumes [4], and an exponential temperature probability distribution (TPD, proportional to the fraction of time that the temperature is within dT of T) at the center of the roll.

While the experiments are necessarily carried out in three-dimensional (3D) cells, preliminary numerical results [6] (including $\mathrm{Nu}-1\propto R^{2/7}$ and exponential TPD's) indicate that the hard-turbulent state exists in 2D. In this Letter we go beyond those preliminary results by presenting quantitative comparisons between extended 2D calculations and the experimental results. The primary limitation of the previous computations [6] is the short nature of the time strings analyzed. In contrast, the present results are computed for over 200 convective time scales ($2\pi/\omega_p$) at each value of R. These time series are taken on a coarse 17×17 submesh of "probes" measuring the temperature and velocity components at least as often as $0.015(2\pi/\omega_p)$. This submesh is horizontally uniform and distributed according to $z_n=-\cos(n\pi/16)$ ($n=0,\ldots,16$) in the vertical. In addition, these simulations are well resolved (computational grid spacings are less than the Kolmogorov length scale [7]).

The numerical method and the development of the 2D "plume" or "blob" instability [8–10] are discussed in the preliminary paper [6]. Here we concentrate on comparison with the experiments. There are several important differences between the experiments and the simulations presented here. First, the experiments are obviously 3D. Second, the experiments have impenetrable, no-slip sidewalls, whereas our solutions have impenetrable, free-slip sidewalls. This simplification speeds the computations at the cost of suppressing a back-roll instability occurring in the corners of the cell [11]. The remaining boundary conditions for our model consist of insulating sidewalls and fixed-temperature, no-slip top and bottom boundaries. Finally, our results are for Prandtl number $\sigma=7$, in contrast to the value $\sigma_{\mathrm{He}}\approx0.7$ for helium [1–3]. We chose this value of σ because time dependence for lower σ occurs at higher R [8], making low-σ computations more costly (viz., periodic time dependence does not set in until $R\gtrsim10^7$ for $\sigma=1$ in 2D).

The fact that the 3D hard-turbulent state is accompanied by a well-defined time scale, $2\pi/\omega_p$, measured at all spatial locations, is surprising when considering the absence of such a signature in the lower-R, soft-turbulent regime [1]. However, visualization of the computed 2D temperature field shows the organization of the flow to be the result of a plume-boundary-layer interplay (i.e., sinking cold plumes born in an unstable region of the upper boundary layer disrupt the lower boundary layer, initiating the formation of hot plumes in the latter). The same process is observed in the 3D visualization experiments of Ref. [4]. In this way, the hard-turbulent flow in the Rayleigh-Bénard cell is organized by the coherent structures to produce a particular time scale.

Figure 1 is a plot of the low-frequency portion of the temporal spectral density obtained just outside the upper and lower boundary layers and also near the sidewalls, where strong plumes are advected; this figure indicates the existence of the coherence frequency ω_p in 2D. Note that as R increases, and both the magnitude and spatial extent of the thermal plumes diminishes, the convective time scale and associated harmonics become less well

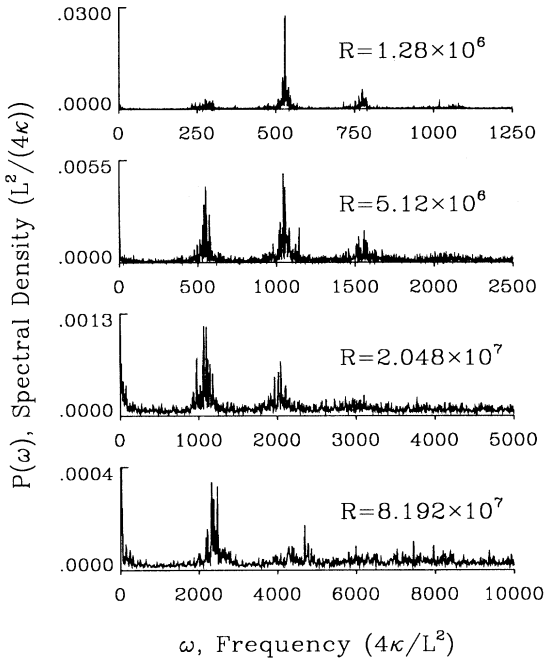

FIG. 1. Spectral density vs Rayleigh number, spatially averaged near the cell boundaries where the ω_p (or one of its harmonics) exhibits a signal-to-noise ratio $\gtrsim 9$. L is the box dimension; κ is the thermal diffusivity. The ω_p peaks nearly line up because the power-law index for ω_p scaling with R is $\sim \frac{1}{2}$.

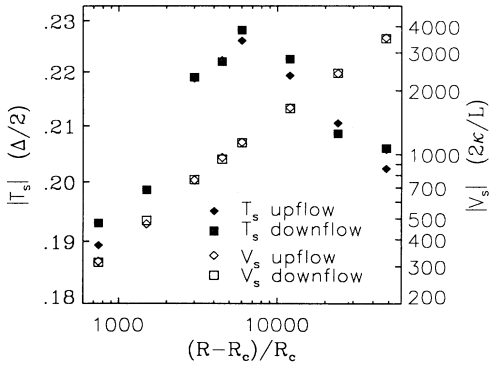

FIG. 2. Transition in the large-scale roll to hard turbulence for sidewall temperature $|T_s|$ (solid symbols) and sidewall velocity $|V_s|$ (open symbols). Note that $\Delta_x = T_s^{up} - T_s^{down}$. Also, $|T_s^{up}| \approx |T_s^{down}|$ and $|V_s^{up}| \approx |V_s^{down}|$ because of the symmetry of the mean roll. Δ is the temperature difference across the box; $R_c = 1708$ is the critical Rayleigh number for our boundary conditions.

defined and the growth of a broad spectral signature becomes apparent. Using $\omega_p \propto R^{\gamma}$, we obtain a scaling exponent of $\gamma_{2D} = 0.518 \pm 0.009$ [12], in good agreement with the experimental result considering that our calculations have free-slip sidewalls and hence have less drag on the mean roll. There is no detectable change in the scaling exponent of ω_p near our transition to hard turbulence, $R_t \approx 1 \times 10^7$, in contrast to the 3D experiments for which no ω_p is observed in the soft-turbulent regime [1]. This is reminiscent of the 2D TPD's, which are exponential in form below the establishment of the 2D hard-turbulent regime [6] even though the 3D experiments produce Gaussian TPD's in soft turbulence. Clearly, soft turbulence, as defined by the 3D experiments, does not exist in 2D at this σ and aspect ratio.

Other signifying features of the large-scale roll, V_s and Δ_x, are depicted in Fig. 2. (Δ_x is the difference in the sidewall temperatures measured at cell midheight.) Both V_s and Δ_x exhibit a decided transition near R_t. Above R_t, the scaling indices obtained are $\delta_{2D} = 0.540 \pm 0.003$ and $\epsilon_{2D} = -0.064 \pm 0.007$ [13], which are different from the experimental values. Though a "correction" in the scaling indices may exist as a result of the change in dimensionality alone, this is difficult to discern from our calculations given the modification of the flow resulting from our simplified sidewall boundary conditions.

Figure 3 depicts Δ_c at the center of the cell versus the reduced Rayleigh number $(R - R_c)/R_c$. The 2D results agree with those obtained from the 3D experiment in the hard-turbulent regime. Whether or not the transition at R_t is manifested in Δ_c cannot be discerned from Fig. 3 because of the relatively large scatter in the data points, which results from the finite length of the time strings coupled with the covariance [14] between different temperatures (viz., measurements made at separate times are *not* statistically independent given the continuous nature of the underlying time string and the existence of the coherence frequency).

A striking signature of the transition does exist, however, in a qualitative change in the temperature skewness [15] of the central region (Fig. 4). Whereas for $R \lesssim 1.024 \times 10^7$ the central part of the roll does not display a discernible *region* in which the skewness is zero, a siz-

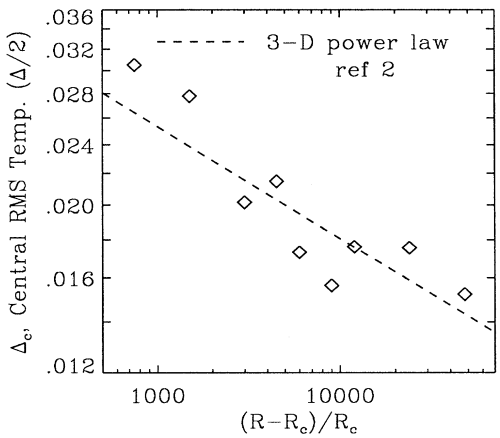

FIG. 3. Central rms temperature vs Rayleigh number. The dashed line is the experimental power law for 3D hard turbulence (arbitrary normalization).

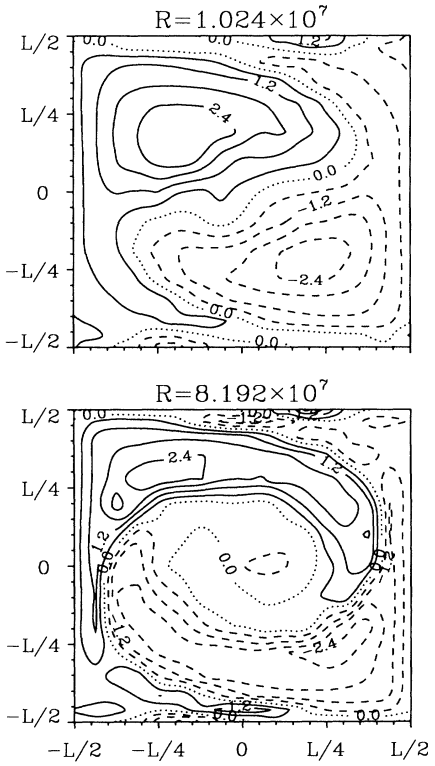

FIG. 4. Temperature skewness, $\langle (T-\langle T\rangle)^3\rangle/T_{\rm rms}^3$. The mean roll rotates clockwise; gravity acts downward. Dotted lines correspond to a skewness of zero. Solid (dashed) lines represent positive (negative) skewness.

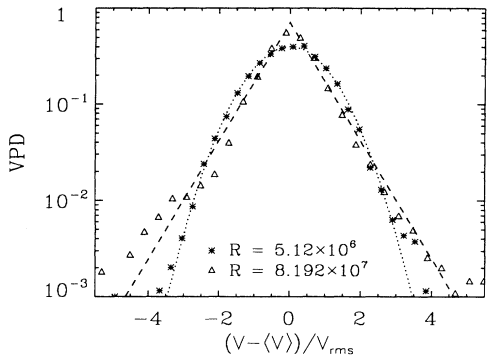

FIG. 5. Velocity probability distribution (VPD) transition. V is the vertical velocity. The VPD for R between 5.12×10^6 and 8.192×10^7 exhibits a continuous transition from Gaussian to exponential form. (These R roughly demarcate the limits of the transition.) Gaussian (dotted) and exponential (dashed) distributions with zero mean and unit variance are shown.

able central region of nearly zero skewness does exist for $R=8.192\times10^7$. A region with zero skewness has a symmetric TPD, signaling equal numbers of hot and cold fluctuations. A large region of zero skewness suggests a well-mixed core, the existence of which is an integral part of the theory put forth by Castaing *et al.* [2].

Finally, we note a transition in the velocity probability distribution (VPD) from a Gaussian to an exponential form in our 2D solutions (Fig. 5). It is not known if such a VPD transition exists in the 3D experiments because there are no instantaneous velocity measurements in the experiments. We find that the 2D VPD transition spans a wider range in R than the corresponding transition at the sidewalls (Fig. 2); however, the range in R spanned by the 2D VPD transition is roughly the same as that for the experimental 3D TPD transition [16]. Further, the existence of this transition in the 2D VPD allows for the test of a conjecture proposed in the previous paper [6], namely, that an exponential TPD might be nothing more than a signal that plumes (i.e., localized structures in the temperature field) are present. If this were the case, the transition to an exponential VPD should be accompanied by the emergence of localized velocity structures. Images of the numerical solutions do not definitively support such speculations. Sharply delineated, coherent structures are clearly visible in both the temperature and velocity fields for $R\gg R_t$; however, weak, diffuse structures are also seen in both fields for $R\ll R_t$, despite the different probability distributions. Further analysis is needed to deduce the relationship between probability distributions and coherent structures.

Summarizing the transition to the hard-turbulent state in our 2D solutions, (1) a qualitative change in the large-scale structure of the flow takes place, including the development of a sizable, "well-mixed" central region exhibiting nearly zero skewness in the temperature field and a change in the scaling of both the mean sidewall velocity and temperature; (2) $\mathrm{Nu}-1$ develops a power-law dependence on R with an exponent consistent with $\frac{2}{7}$; and (3) the VPD undergoes a transition to an exponential-like form. Further, while the 2D results exhibit power laws for both ω_p and Δ_c and an exponential TPD as do the 3D experiments in hard turbulence, these features are present below R_t and, hence, the 2D calculations are unable to duplicate the behavior of soft turbulence. We believe that this departure from the experimental results for $R<R_t$ is rooted in the boundary conditions of our model. Our boundary conditions, both the free-slip sidewalls and the 2D geometry, suppress many of the early instabilities that lead to time dependence in thermal convection [6,8–11]. The first realizable instability from the steady-roll state is the one which results in plumes and, as a result, we are able to observe the progression of this flow as it develops from the linear "blob" instability [8]. That a characteristic frequency at ω_p and the exponential TPD for $R<R_t$ is a *direct* consequence of plumes is not established. Indeed, these features may result from some *other* product of the constraints on the flow.

For $R>R_t$, the duplication of many of the features of

hard turbulence in 2D raises the question: Can we learn something about 3D flow by studying 2D numerical flows? Indeed, despite the fact that the 3D experiments report a robust mean roll, which is basically a 2D entity, 2D and 3D turbulent flows are fundamentally different on the smallest scales [17]. Furthermore, simulations in 3D clearly demonstrate the 3D morphology of the plumes themselves [18]. Nevertheless, despite these obvious differences between 2D and 3D flows, these very features—the dimensionality-dependent geometry of plumes and the smallest-scale motions—apparently play a minor role in determining the aspects of hard turbulence considered here. As a result, some properties of hard turbulence, such as the scaling of $\mathrm{Nu}-1$ on R, are recovered theoretically from a variety of models [2, 19,20], none of which depend crucially on a detailed treatment of plumes and none of which is fundamentally 3D.

In summary, we have demonstrated that the hard-turbulent state exists in 2D flow. Not only is the qualitative picture of a robust roll dominated by plumes borne out by our 2D solutions, but excellent quantitative agreement between our 2D calculations and the 3D experiments is obtained for both the power-law indices for the Nu and Δ_c scaling on R and the exponential form of the TPD. The scaling index for ω_p is in fair agreement considering the reduced drag imposed on the mean roll by our free-slip sidewalls. Furthermore, the quantities whose scaling on R does not agree, V_s and Δ_x, are precisely those obtained at these idealized sidewalls. In addition, our solutions show that the transition to 2D hard turbulence is accompanied by a transition in the VPD and the development of a sizable, central region with an unskewed TPD; it is not known if such changes accompany the 3D transition. We will continue to explore the behavior of this 2D model in the hope that it will shed some light on the 3D hard-turbulent state.

We would like to acknowledge engaging discussions with G. Fisher, M. Leibig, and X. Z. Wu. We appreciate comments on our work by A. Libchaber. This work was supported in part by the NASA Space Physics Theory Program at The University of Chicago and Air Force Grant No. AFOSR 90-0116 to the University of Hawaii.

[1] F. Heslot, B. Castaing, and A. Libchaber, Phys. Rev. A **36**, 5870 (1987).
[2] B. Castaing, G. Gunaratne, F. Heslot, L. Kadanoff, A. Libchaber, S. Thomae, X. Z. Wu, S. Zaleski, and G. Zanetti, J. Fluid Mech. **204**, 1 (1989).
[3] M. Sano, X. Z. Wu, and A. Libchaber, Phys. Rev. A **40**, 6421 (1989).
[4] G. Zocchi, E. Moses, and A. Libchaber, Physica (Amsterdam) **166A**, 387 (1990).
[5] W. V. R. Malkus and G. Veronis, J. Fluid Mech. **4**, 225 (1958).
[6] E. E. DeLuca, J. Werne, R. Rosner, and F. Cattaneo, Phys. Rev. Lett. **64**, 2370 (1990).
[7] A. N. Kolmogorov, C. R. Acad. Sci. URSS **30**, 301 (1941).
[8] E. W. Bolton, F. H. Busse, and R. M. Clever, J. Fluid Mech. **164**, 469 (1986).
[9] D. R. Moore and N. O. Weiss, J. Fluid Mech. **58**, 289 (1973).
[10] T. B. Lennie, D. P. McKenzie, D. R. Moore, and N. O. Weiss, J. Fluid Mech. **188**, 47 (1988).
[11] I. Goldhirsch, R. B. Pelz, and S. A. Orszag, J. Fluid Mech. **199**, 1 (1989).
[12] The uncertainty in γ_{2D} is estimated from the fit. The uncertainty in ω_p used is the peak half width at half maximum obtained from Fig. 1.
[13] The uncertainty in the index is obtained by a least-squares fit to the data. The uncertainty in the raw data is estimated from the scatter in the data.
[14] P. R. Bevington, *Data Reduction and Error Analysis for the Physical Sciences* (McGraw-Hill, New York, 1969), p. 59.
[15] The skewness of a time string, A, is defined by $\langle (A-\langle A\rangle)^3\rangle / A_{\mathrm{rms}}^3$, where $\langle A\rangle$ denotes the temporal mean of A and A_{rms} is the root-mean-squared value of A.
[16] X. Z. Wu (private communication).
[17] R. H. Kraichnan and D. Montgomery, Rep. Prog. Phys. **43**, 547 (1980).
[18] J. R. Herring and J. C. Wyngaard, in *Turbulent Shear Flows*, edited by F. Durst, B. F. Launder, F. Schmidt, and J. H. Whitelaw (Springer-Verlag, Berlin, 1987), Vol. 5, p. 324.
[19] G. O. Roberts, Geophys. Astrophys. Fluid Dyn. **12**, 235 (1979).
[20] B. I. Shraiman and E. D. Siggia, Phys. Rev. A **42**, 3650 (1990).